

A New Experimental Approach to the Influence of Pore Geometry on Laboratory Water-Oil Relative Permeability and Oil Recovery Using A Reconstituted Matrix Based on Sand and Clay Particles

Zakaria Adjou¹, Djamila Boufades¹, Zahaf Maamar¹, Belahlou Narimene¹, Mustapha Miloudi¹, Souad Hammadou née Mesdour²

¹ Department of Hydrocarbon Production, KasdiMerbah University, Ouargla, Algeria

² Laboratory of Applied Chemistry and Materials (LabCAM), University of M'hamed Bougara of Boumerdes, Avenue de l'Indépendance Boumerdes, Algeria

Received October 10, 2024; Accepted December 17, 2024

Abstract

Pore geometry affects the water-oil relative permeability and oil recovery efficiency by determining the preferential pathways taken by fluids in the porous medium. This study examines the impact of pore geometry on three different sized homogeneous and heterogeneous samples based on sand and sand with 20% clay on laboratory-measured porosity, relative permeability, and oil recovery. Every experiment was carried out in a laboratory setting. The oil relative permeability varied according to the results, increasing with grain size (0.643D for 500 μm , 0.535D for 250 μm , 0.503D for 125 μm , and 0.654D for the polymodal sample). The polymodal sample also showed a drop in oil relative permeability from 0.654D to 0.510D because of the presence of clay. Thirteen milliliters (13 ml) of additional oil were found in the polymodal sample. The work's findings can help make decisions that will enhance oil recovery and enhance our understanding of the preferred pathways taken by fluids in extremely heterogeneous reservoir rocks.

Keywords: Pore geometry; grain size, polymodal medium; preferential pathway; relative permeability; oil recovery.

1. Introduction

Multiple natural and industrial processes involve multiphase flow in porous medium [1-2]. It is crucial to comprehend the pore-scale fluid displacement in these processes, as it is influenced by pore geometry [3]. Recently, multiphase flow in porous medium has been studied by combining sample flooding experiments with pore geometry evaluation [4-5]. Pore geometry, grain sizes distribution and topology are the main factors influencing relative permeability behavior. Predicting the behavior of oil-water flow in complex rocks with wide pore size distributions is particularly challenging [6-8]. Prior experimental investigations at the pore scale have predominantly focused on multiphase flow in homogeneous sandstone formations characterized by unimodal pore size distributions [9-10]. Only a limited number of experimental works exist on intricate rock's grain geometries, particularly those frequently observed in carbonates [11-12]. For complex porous medium, mainly increase water saturation reduces relative permeability [13-14]; the influence of geometry can vary significantly, particularly due to the interaction between flow through microporosity and macropores. Moreover, the relative permeability in all these works has not been comprehensively evaluated concerning measurement uncertainty [15]. Therefore, our work differs from previous research in that it uses a new experimental approach of complex reconstituted matrix based on sand and clay particles and simultaneous oil-water injection to evaluate multiphase flow permeability's and the incremental oil volume recovered in order to prove the relationship between pore geometry distribution

and its effect on oil-water relative permeability. The results of the study support better decision-making when it comes to the use of secondary recuperation by water flooding or gas flooding in order to avoid oil retention in the porous medium due to pore geometry distribution.

2. Materials and methods

2.1. Sand

Hassi Messaoud sandstone formations are characterized by good porosity and permeability properties. Hydrocarbons in Hassi Messaoud's reservoir rocks consist of a mixture of common oil and natural gas. We formed sand samples with three different grain sizes for various studies such as porosity and permeability measurements, grain size analysis, fluid saturation studies, and rock-fluid interactions. In addition, sand is known for its sensitivity to water, which makes it easier to put in place in general.

The sample was identified by two principal analysis conducted in the University Scientific and Technical Research Center for Physical and Chemical Analysis (CRAPC):

SEM (Scanning Electron Microscopy): enables high-resolution imaging at magnifications ranging from a few times to several hundred thousand times of the surface morphology of geological samples. It offers comprehensive details on characteristics like texture, shape, and size of the grain.

EDX (Energy Dispersive X-ray Spectroscopy): When analyzing the elemental composition of geological samples, EDX offers both qualitative and quantitative information. It helps in mineral identification, elemental distribution mapping, and the comprehension of geological processes by being able to detect and measure the presence of different elements.

2.2. Brine

The brine used in all of the trials was created in the laboratory. To make this brine, dissolve 250g of NaCl in 1 liter of distilled water. This brine is utilized for the liquid/liquid displacements of the samples during the drainage and imbibitions tests.

2.3. Diesel

The diesel was used as oil in all monophasic and diphasic flow experiments, as well as imbibitions tests. Table 1 displays diesel's characteristics.

Table 1. Properties of gasoil.

Density at 15°C	0.828 g/cm ³	Pour point	- 14°C
Dynamic viscosity at 20°C	5.6 mPa s	Initial boiling point	152°C
Surface tension at 20°C	30 mN/m	Final boiling point	320°C
Flash point	88°C		

2.4. Clay

Clay is a type of fine-grained sedimentary material consisting of very small mineral particles, it can act as a sealant or barrier in geological formations, affecting fluid flow properties such as permeability, the clay used in the experiences was also identified by the SEM and EDX methods.

3. Experimental procedures

3.1. Sample preparation

The experiments were carried out on sand samples. Prior to use, the sand sample undergoes different preparative steps as shown in Figure 1 as follows:

Washing: sand sample is washed in order to remove fine particles and impurities that could affect experimental results by clogging spaces between sand grains.

Drying: after washing, the sand was dried to ensure consistent moisture content, preventing interference with the measurements. Essentially, it's about ensuring the sand sample is clean and uniform to conduct accurate measurements.



Figure 1. The used sample sand undergoes sequential preparation tests.

Sieving: the objective is to segregate the sand sample into distinct particle size fractions that aids in the identification and collection of sand particles of specific diameters, that essential for subsequent analysis of each diameter in our experiment process; sand sample underwent sieving using a HAVER BOEKHER type D-59302 OELDE sieve shaker. Initially, the sieves were positioned within the sieve shaker. Subsequently, the instrument was activated, with due consideration given to the configuration of key parameters. Specifically, the agitation mode was set to continuous agitation, accompanied by agitation amplitude of 2500 pulses per minute, and agitation duration of 5 to 10 minutes. Once these parameters were meticulously adjusted, the sand sample was introduced into the topmost sieve column. Finally, the instrument was activated by engaging the on/off button, commencing the sieving operation with a methodological rigor and experimental precision.

Fractions collection and weighing: following sieving, sand fractions corresponding to discrete diameters were meticulously collected. Each fraction underwent mass determination using a precision balance to ascertain its weight accurately.

Cumulative assessment: the weights of sand fractions were used to compute cumulative weights for distinct diameters, contributing to the establishment of a comprehensive dataset. of particular focus were diameters measuring 500 micrometers, 250 micrometers, and 125 micrometers, identified for inclusion in forthcoming experimental investigations.

Sand-clay sample preparation: a quantity of 20% of clay is added to some of the same chosen sand grain's diameters to form a heterogeneous sample. Sand with 20 % clay (The majority of Hassi Messaoud's petroleum reservoirs contain from 15% to 30% of clay).

3.2. Designed sand-based micromodels

Diameters of 500, 250, and 125 micrometers will be separately inserted into cylindrical cells with diameters of 2.15 cm and a length of 9.3 cm. Because of this varied arrangement, the particle distribution inside the micromodels can be visualized and examined, providing insights or simulation of porous media of rock reservoirs and their variety influence on its properties. Furthermore, by integrating all three diameters into a single cellule, a composite micromodel will be created.

3.3. Oil recovery determination tests

Commence the saturation process of the micromodel by introducing brine into the system, establishing initial conditions where the porous medium exhibits 100% water saturation (Figure 2). Inject oil to displace the brine until the first drop of oil is recovered. The primary objective at

this stage is to achieve irreducible water saturation (S_{wi}). Determine the volume of oil saturation within the system, indicating the amount of oil present in place. Imbibe the system by reinjection of brine. Cease brine injection upon recovery of the first drop of brine.

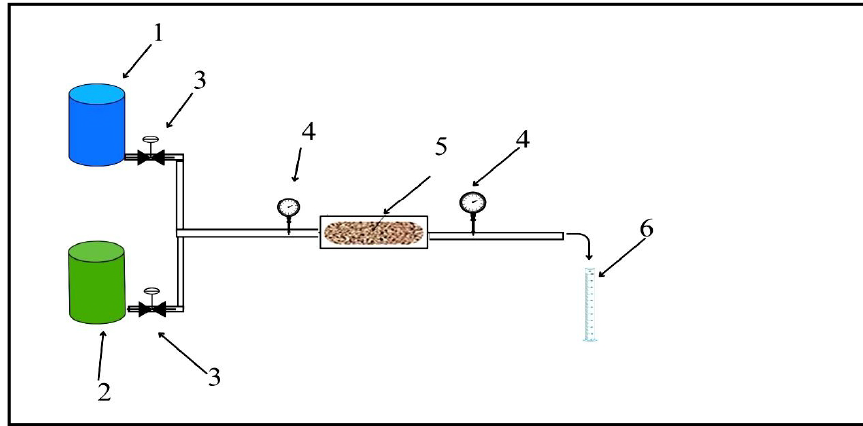


Figure 2. Drainage and imbibitions installation: (1) water injection reservoir, (2) oil injection reservoir, (3) valves, (4) manometers, (5) sample core holder, (6) graduated cylinder.

Measure the volume of oil recovered collected in the graduated cylinder. Calculate the volume of residual oil by:

$$V_{or} = OOIP - V_r \quad (1)$$

where V_{or} the residual oil volume (mL); $OOIP$ is the original oil in place (mL); and V_r is the recovered oil volume (mL).

3.4. Porosity measurements

Porosity is measured by weighing the dry samples of each dimension across three tests, which is then completely saturated with brine after minor compaction of sand. Porosity is determined by [16]:

$$\phi = \frac{m_s - m_d}{m_s} \quad (2)$$

where ϕ is porosity (%); m_s is the saturated mass (g); and m_d is the dry mass (g).

The same procedure was applied for measuring the porosity of a sample containing clay.

3.5. Permeability measurements

Absolute permeability: the absolute permeability of the aqueous and oil phases is determined following sample preparation with the three different grain sizes and the polymodal. Subsequently, applying Darcy's law allows the calculation of the absolute permeability values for both phases:

$$Q = \frac{K_a A}{\mu} \times \frac{\Delta P}{L} \quad (3)$$

where Q is the flow rate of the phase through the sample (cm^3/s); K_a is the absolute permeability of the flowing phase (Darcy); A is the fluid passage section (cm^2); μ is representing fluid viscosity (cP); ΔP is the differential pressure (atm); and L is the length of the sample (cm). Noting that K_{ao} and K_{aw} are absolute permeability of oil and water respectively (Darcy).

Effective permeability: a displacement approach was applied to determine the effective permeability. It is conducted at 25°C and across varying pressure levels, the experiment subsequently entails measuring effective permeability across four samples (each for different grain sizes and one for the polymodal sample). The procedure initiates with saturating the sample with brine (100%) for water effective permeability measurement and with oil for oil effective permeability. Then, oil is used to drain the brine from the sample until irreducible brine saturation (S_{wi}) is achieved. Brine is used to imbibe the oil from the samples until residual

oil saturation is achieved. Finally, both oil (K_{eo}) and water effective permeability (K_{ew}) at different pressure levels are determined according to the generalized Darcy's law:

$$Q_o = \frac{K_{eo} \cdot A}{\mu_o \cdot L} \cdot \Delta P_o \quad (4)$$

$$Q_w = \frac{K_{ew} \cdot A}{\mu_w \cdot L} \cdot \Delta P_w \quad (5)$$

where Q_o is the volumetric oil flow rate (cm^3/s); Q_w is the volumetric water flow rate (cm^3/s); K_{eo} and K_{ew} are the effective permeability of oil and brine respectively (mD); μ_o and μ_w are oil and water viscosity respectively (cP); L is the length of the sample (cm); A is the fluid passage section (cm^2); and ΔP_o and ΔP_w are the differential pressures applied for oil and brine respectively (atm).

Relative permeability: Relative permeability of oil and brine was determined by:

$$K_{ro} = \frac{K_{eo}}{K_{ao}} \quad (6)$$

$$K_{rw} = \frac{K_{ew}}{K_{aw}} \quad (7)$$

where K_{rw} and K_{ro} are the relative permeability of brine and oil respectively (mD).

For the sample containing sand and clay, absolute, effective, and relative permeability brine and oil were carried out by applying the same previous procedures.

4. Results and discussion

4.1. Sand particles analysis results

SEM imaging results: all the SEM analysis imaging results of 500 μm , 250 μm , and 125 μm sand's grain sizes, the polymodel medium, and clay are presented in Figures 3, 4, 5, 6, 7, and 8, respectively.

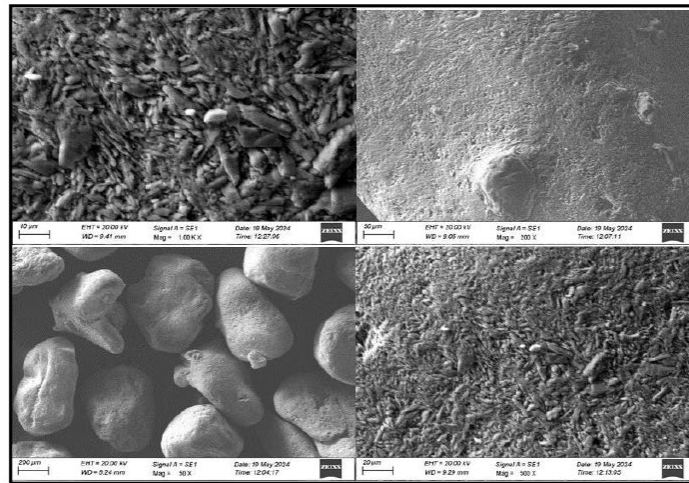


Figure 3. SEM imaging results of 500 μm grain size magnified at 50x, 200x, 500x, 1000x.

For the 500 μm :

50X magnification: the grains appear well-rounded and relatively smooth. There are visible intergranular spaces. 200X magnification: surface texture of the grains starts to show more details, revealing minor irregularities and some fine particles adhering to larger grains. 500X magnification: surface roughness is evident with the appearance of micro-pores and surface cracks. 1.00KX magnification: detailed observation of the grain surfaces shows distinct micro-structures, with noticeable porosity and surface texture irregularities.

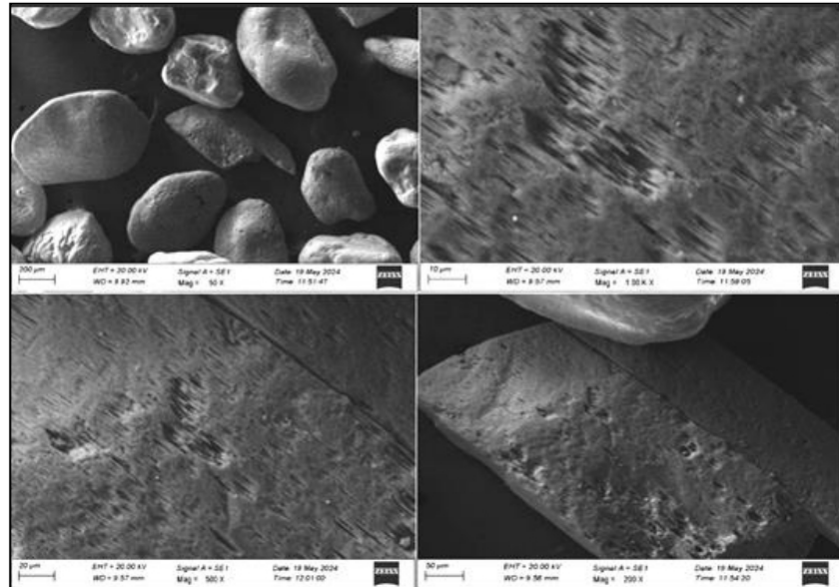


Figure 4. SEM imaging results of 250µm grain size magnified at 50x, 200x, 500x 1000x.

For the 250 µm:

50X magnification: grains are smaller and appear more angular compared to 500µm grains. Intergranular spaces are reduced. 200X magnification: surface texture reveals more pronounced angularity and roughness. Fine particles are seen clinging to the surfaces. 500X magnification: the surface structure is more complex, with visible micro-cracks and rough texture. 1.00KX magnification: high magnification reveals intricate surface details, with significant roughness and microstructural features.

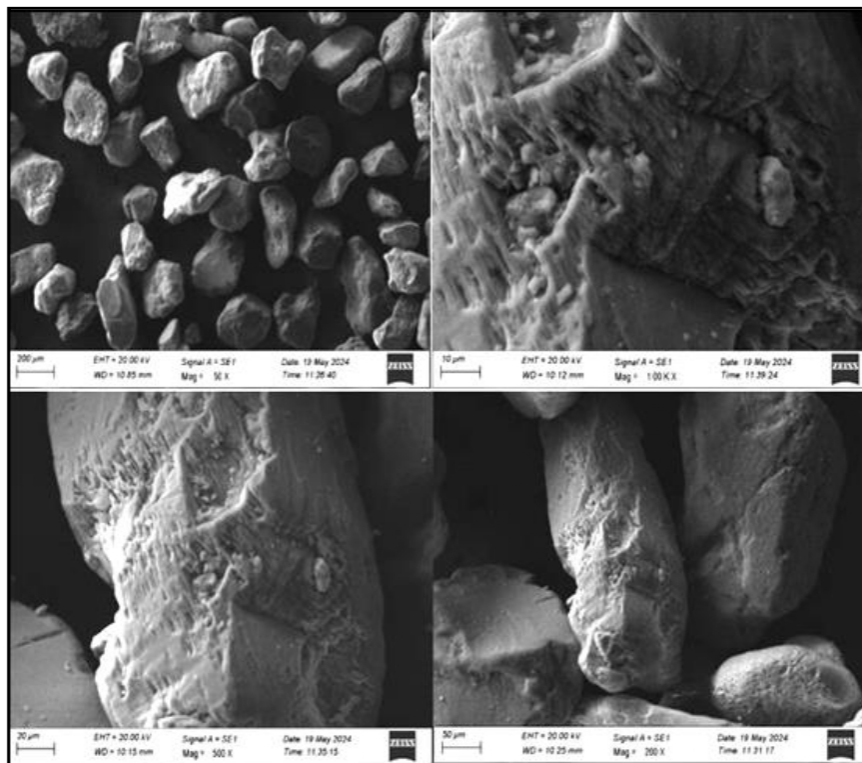


Figure 5. SEM imaging results of 125µm grain size magnified at 50x, 200x, 500x 1000x.

For the 125 μm :

50X magnification: grains are much smaller and appear very angular. The packing density seems higher due to smaller grain size. 200X magnification: the surface texture is highly irregular with sharp edge sand rough surfaces. 500X magnification: detailed surface features show significant angularity, with more visible cracks and pores. 1.00KX magnification: the microstructure is very complex, with highly detailed surface irregularities and a rough texture.

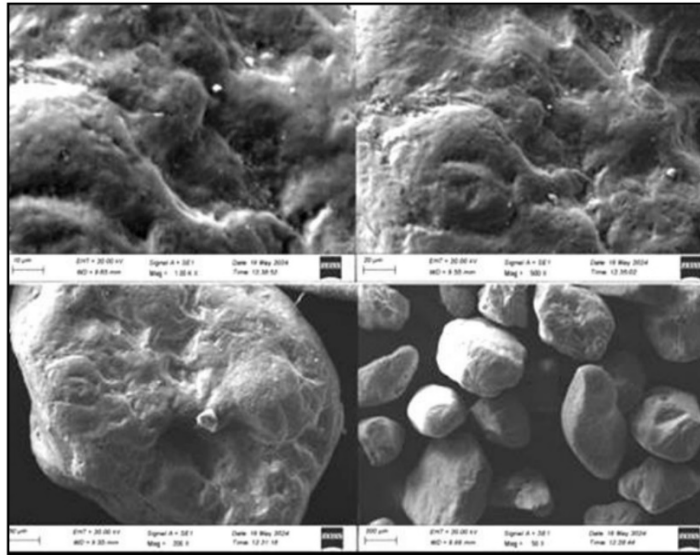


Figure 6. SEM imaging results of polymodal medium magnified at 50x, 200x, 500x 1000x.

For the polymodal medium:

50X magnification: variety of grain sizes and shapes are visible, indicating a polymodal distribution. Grains appear densely packed. 200X magnification: surface textures of different grains show varying degrees of roughness and irregularities. 500X magnification: individual grains reveal complex surface structures with visible micro-cracks and pores. 1.00KX magnification: high magnification shows intricate details of the surface morphology, with significant porosity and surface texture variations among different grains.

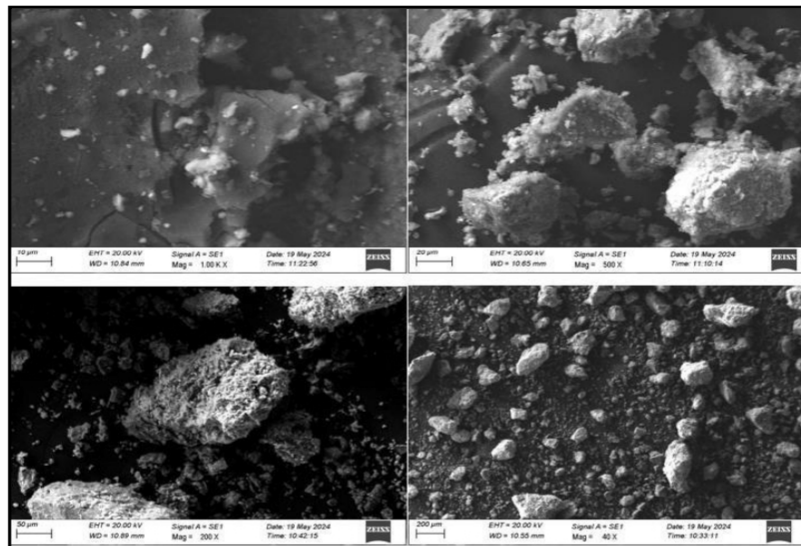


Figure 7. SEM analysis imaging of clay magnified at 50x, 200x, 500x 1000x.

For the clay:

50X magnification: clay particles appear very fine and densely packed. The surface is smooth at this magnification. 200X magnification: details of the clay particle surfaces are visible, showing minor roughness and fine aggregates. 500X magnification: the surface texture is more apparent, revealing micro-cracks and slight porosity. 1.00KX magnification: high magnification shows detailed microstructural features of the clay particles, including significant porosity and intricate surface irregularities.

SEM imaging results: after performing the EDX analysis, the analytic results show that sand containing minerals such as significant quantity of Si, S, Ca, Mg, and Al as shown in Figure 8, and that clay contains Fe, K, Ca, Mg, and Al as shown in Figure 9.

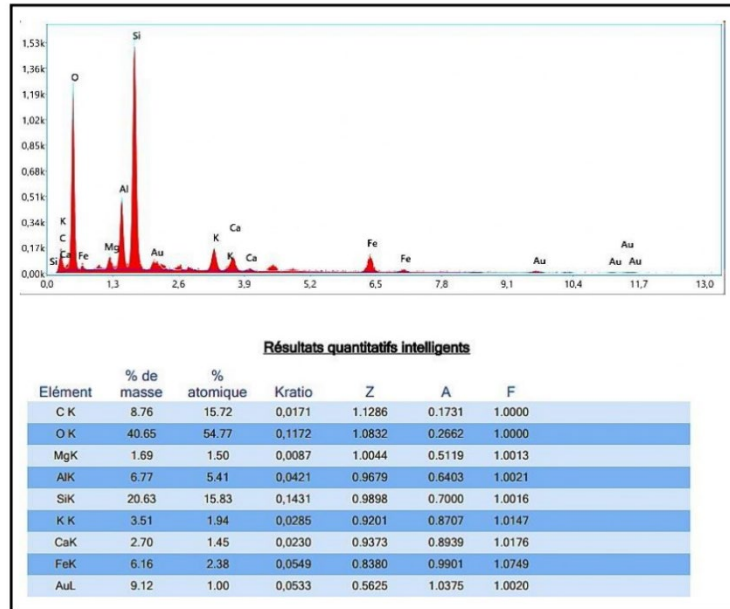


Figure 8. Energy dispersive X-ray spectroscopy results of sand.

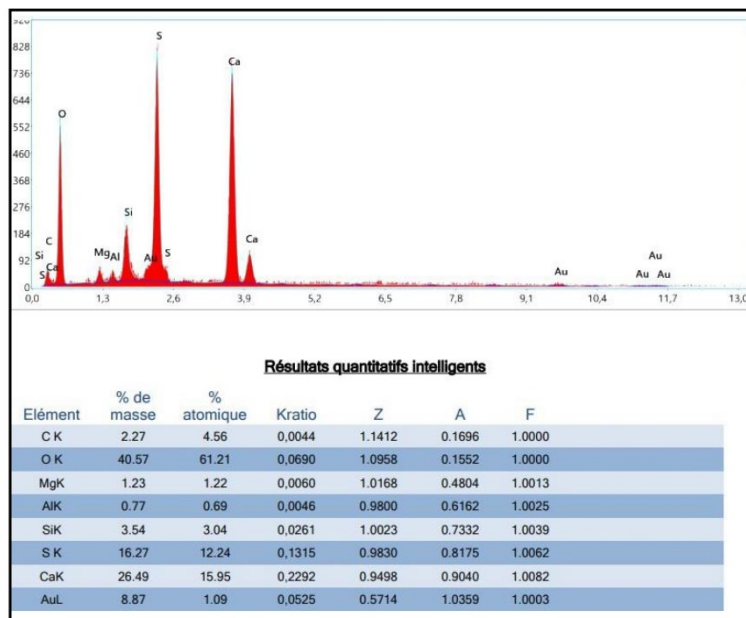


Figure 9. Energy dispersive X-ray spectroscopy results of clay.

Granulometric analysis results: from the different segregated sizes (Table 2) an intermediate range within the interval [125- 500] μm was chosen to obtain an average permeability value. The largest particles [1000 - 2000] μm give high permeability values. The finest particles [45-90] μm were eliminated as they obstruct the passage of fluids through the pipes and filter paper in the experimental liquid/liquid displacement device.

Table 2. Granulometric sand analysis results.

Sieve diameter (μm)	Mass (g)	Not cumulative (%)	Cumulative (%)
2000	0.2	0.02	99.98
1250	0.1	0.01	99.97
1000	4	0.4	99.57
500	346.5	34.65	64.92
250	502.2	50.22	14.7
125	120.8	12.02	2.68
90	17.2	1.72	0.96
63	1.9	0.19	0.77
45	0.1	0.01	0.76

4.2. Oil recovery results

The OOIP, the recovered oil volume, and the residual oil volume are based on the drainage and imbibitions results, which are presented in Tables 3 and 4, respectively. According to the results, the polymodal medium presents a high recovered oil volume of 13 ml from 19 mL of the OOIP in comparison with the other samples. This result can be explained by the heterogeneity of the sample in which oil can be produced through different intergranular pathways.

Table 3. Drainage by oil results.

Differential pressure (atm)	OOIP (mL)			
	500 μm	250 μm	125 μm	Polymodal
1.0049	20	18	17.5	16
1.0098	21.5	18.5	18	17
1.0147	22.25	18.5	18	17.75
1.01962	22.5	20	18.5	18.5
1.024525	22	22	20.5	19

Table 4. Imbibition by brine results.

Differential pressure (atm)	Recovered oil volume (mL)				Residual oil volume (mL)			
	500 μm	250 μm	125 μm	Poly-modal	500 μm	250 μm	125 μm	Poly-modal
1.00490	13	10	10	10	7	8	7.5	6
1.00891	14	10.5	11	9.75	7.5	8	7	7.25
1.01470	13	13	11.5	12	9.25	5.5	6.5	11.75
1.01962	14	12	9	10	8.5	8	9.5	8.5
1.02453	14	13.75	12	13	8	8.25	8.5	9.25

4.3. Porosity results

Samples of each chosen size and a mixture of them representing the heterogeneous medium (polymodal) and others mixed with clay are saturated with brine, and measurements of their dry mass (before saturation) and saturated mass are performed repeatedly to prove the accuracy of the data obtained. The results are shown in Tables 5, 6, 7 and 8. The results illustrate a clear relationship between grain size and porosity in both monomodal and polymodal samples.

Monomodal samples: larger grains typically have fewer and larger pore gaps, reducing overall porosity. The porosity increases as the grain size decreases. Smaller grains pack more tightly, creating larger pore spaces per unit volume. The smallest grain size measured has the maximum porosity, as they have a larger surface area to volume ratio, allowing for more

empty spaces inside a given volume. Due to their ability to form densely packed structures with multiple tiny spaces.

Table 5. Porosity results of 500µm grain size.

Test	Dry mass (g)	Saturated mass (g)	Porosity (%)
01	255.400	284.419	10.2
02	254.364	283.792	10.3
03	252.278	285.804	11.7
Average=10.73%			

Table 6. Porosity results of 250µm grain size.

Test	Dry mass (g)	Saturated mass (g)	Porosity (%)
01	255.375	287.254	11.09
02	255.513	289.735	11.8
03	252.843	287.388	12
Average=11.63%			

Table 7. Porosity results of 250µm grain size.

Test	Dry mass (g)	Saturated mass (g)	Porosity (%)
01	249.900	283.209	11.76
02	247.325	282.390	12.4
03	250.402	283.411	11.7
Average=11.95%			

Table 8. Porosity results of the polymodal sample.

Test	Dry mass (g)	Saturated mass (g)	Porosity (%)
01	253.248	284.75	11.06
02	257.99	287.28	10.19
03	255.208	285.128	10.49
Average=10.58%			

The polymodal sample demonstrated a lower porosity compared to the individual grain sizes. This is because the mixture of different sizes allows smaller grains to occupy the spaces between larger grains, thereby reducing overall porosity. This filling effect decreases the total volume of voids within the sample.

4.4. Effect of clay on porosity results

The porosity of the polymodal sample differs noticeably from 10.63% to 10.15% (Table 9) as a result of the presence of clay. The smaller pore spaces between the sand grains are typically occupied by clay particles, which are much smaller than the sand grains. Decreasing the pore volume and total storage capacity when some of the interstitial gaps that would normally contribute to porosity are filled and blocked by clay. While its contribution may appear minor, it can have a significant impact on large-scale reservoir performance.

Table 9. Porosity results of the heterogeneous sand with clay sample.

Test	Dry mass (g)	Saturated mass (g)	Porosity (%)
01	248.70	280.395	10.5
02	252.247	280.790	10.56
03	259.86	285.530	9.4
Average=10.15%			

4.5. Absolute permeability results

Absolute permeability results are shown in Figures 10 and 11 for the heterogeneous polymodal sample. The obtained results show that the heterogeneous polymodal sample had a lower permeability to water (0.40 Darcy) than oil (0.45 Darcy), despite the oil test being conducted at a slightly higher differential pressure. This shows that the sample's structure makes oil flow more easily than water. The inclusion of clay most likely contributes to this discrepancy since it is more hydrophilic, allowing for better oil flow while potentially restricting water flow due to finer particle sand increasing capillary force. As a result, clay reduces water permeability more than oil permeability.

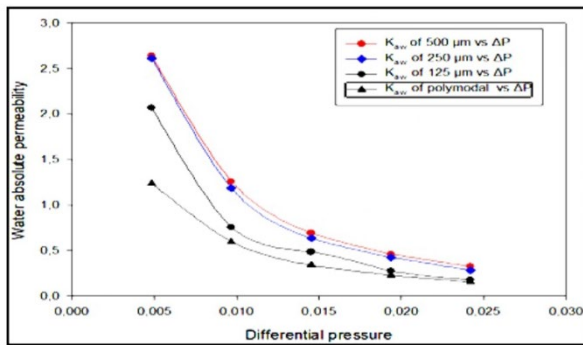


Figure 10. Water absolute permeability as a function of differential pressure

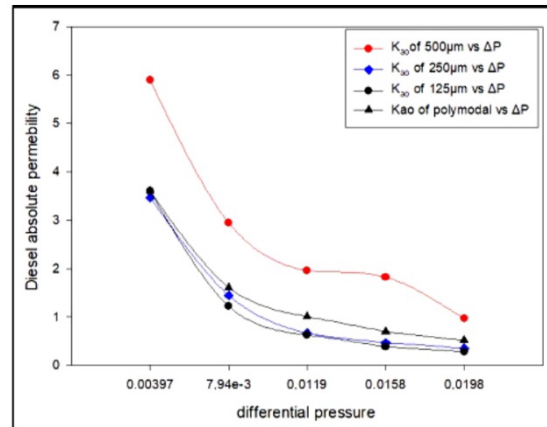


Figure 11. Oil absolute permeability as a function of differential pressure.

4.6. Effective permeability results

Effective permeability results are shown in Figures 12, 13, and 14. The curves demonstrate that permeability's in sandstone decreases with increasing differential pressure across several grain sizes and a polymodal distribution.

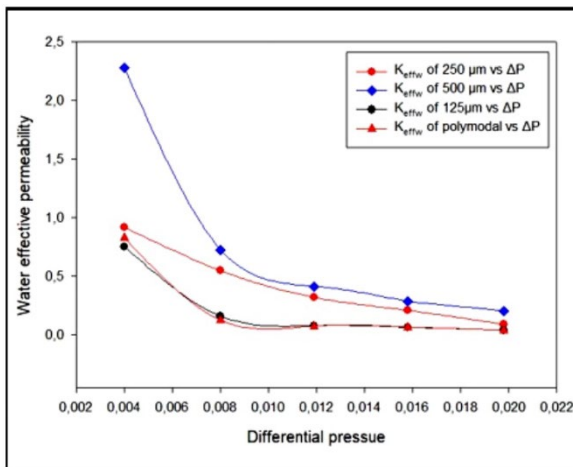


Figure 12. Water effective permeability as a function of differential pressure.

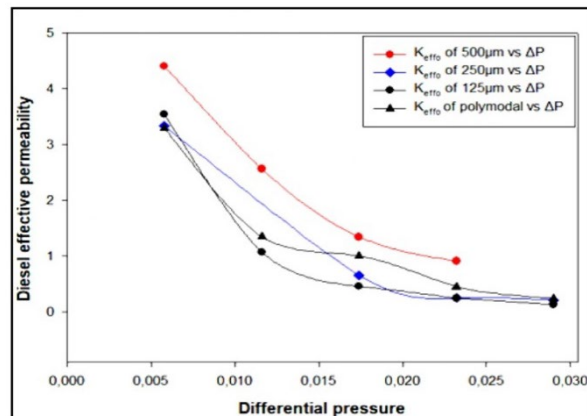


Figure 13. Oil effective permeability as a function of differential pressure.

Permeability of both fluids is initially higher for larger grain sizes (500μm and 250μm), this is because larger pores offer less resistance to fluid flow. The 125μm grain size has the lowest

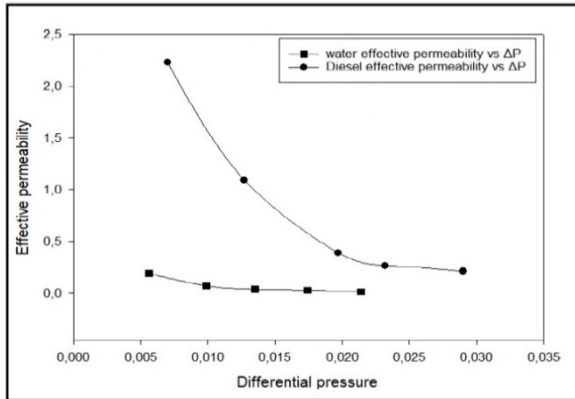


Figure 14. Both, oil and water effective permeability's in presence of clay as a function differential pressure.

effective permeability among the three uniform grain sizes; this could be due to the fact that smaller pores are more easily compressed under pressure, reducing permeability more significantly. The mix of grain sizes likely results in more complex pore structures, which can impede flow more than uniformly larger grains, leading to lower permeability in the heterogeneous mixture compared to individual grain size. Grain size reduction exhibits more significant permeability reduction for oil than to water due to its higher viscosity.

The sandstone's clay particles function as microscopic barriers, drastically decreasing the size of the pores between the sand grains. Fluid flow is restricted by this reduction in pore size.

Since oil doesn't react with clay as strongly as it does with water, it is less restricted and its effective permeability is reduced less than that of water.

4.7. Relative permeability results

Relative permeability results are shown in Figure 15. Smaller pores restrict water flow due to capillary trapping, leading to a decrease in water relative permeability with decreasing pore volume. Conversely, larger pores favor oil flow by providing more connected pathways as water drains from them, resulting in an increase in oil relative permeability with decreasing pore volume. The polymodal sample, with a distribution of grain sizes, offers a more complex pore network. While it contains smaller pores that can trap water, it also possesses larger pores, thus creating a more favorable network for oil flow compared to the individual grain size samples, leading to the observed curves in relative permeability.

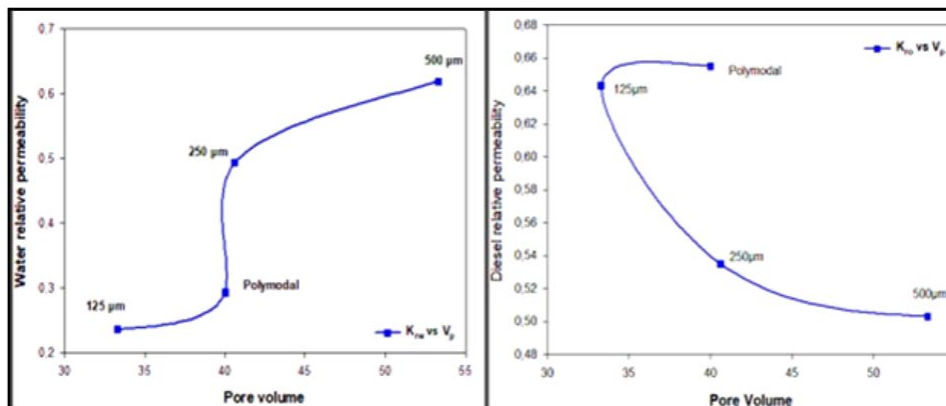


Figure 15. Evolution of oil-water relative permeability's as a function of pore volume.

Relative permeability for both oil and water as a function of water saturation are shown in Figures 16, 17, 18, 19. The relative permeability of water (K_{rw}) increases with water saturation, while the relative permeability of oil (K_{ro}) decreases. This is because water occupies the smaller pores first, hindering the flow of oil. Medium grain sizes (250 μm) show more gradual permeability changes, indicating a balance between fluid pathways, while smaller grain sizes (125 μm) typically correspond to lower permeability due to a higher flow resistance caused by narrower pore throats with less risk of early breakthrough, though mobilizing then on-wetting phase (oil) could be more challenging. While the larger 500 μm curve indicates rapid changes

and high end- point permeability's, suggesting strong preferential pathways and quick fluid displacement but potentially leading to an early breakthrough.

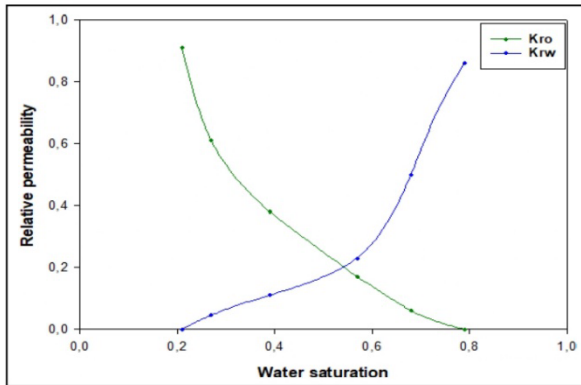


Figure 16. Oil-water permeability's as function of water saturation (500µm).

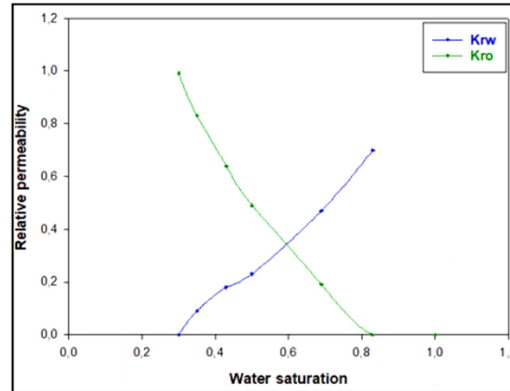


Figure 17. Oil-water permeability's as function of water saturation (250µm).

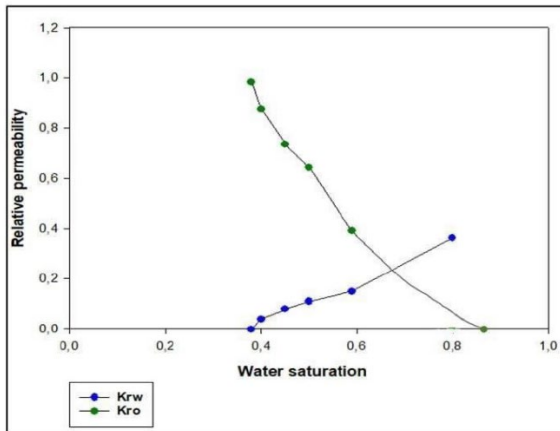


Figure 18. Oil water permeability's as a function of water saturation.

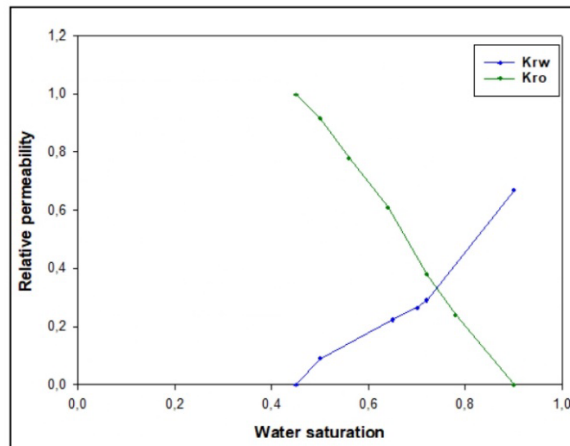


Figure 19. Oil-water permeability's as function of water saturation for heterogenous sample.

The curve for the heterogeneous mixture exhibits a more gradual change in relative permeability due to the variation in pore throat sizes. K_{rw} shows a sharp increase from S_{wi} , indicating rapid mobilization of water once it surpasses the initial saturation threshold, while K_{ro} shows a steady decline, suggesting oil is gradually displaced by water.

The irreducible water saturation (S_{wi}) also increased with decreasing grain size: 21% for the 500µm size, 30% for 250µm, and 38% for the size of 125 µm, indicating that finer pores trap more water even at high oil flow rates due to stronger capillary forces. The residual oil saturation typically occurs at higher water saturations in smaller grains, reflecting the increased difficulty in displacing oil as grain size decreases, as finer grains (125µm) exhibited lower residual oil saturation compared to coarse grains.

While water has a higher mobility, the cross over will occur at water saturation more than 0.5 oil occupies the large-size pores and will therefore be produced. This phenomenon is explained by the Jamin effect. The intersection points shifted to higher water saturations with decreasing grain size: 0.45 Darcy for 500 µm, 0.55 Darcy for 250 µm, and 0.65 Darcy for 125 µm. This indicates that finer grains trap more water and retain less oil, requiring higher water saturations for water permeability to equal oil permeability.

5. Conclusions

This work developed new experimental approach for studying and simulating oil-water relative permeability based on reconstituted matrix mainly made of sand and clay particles to predict pore geometry distribution effect on relative permeability of oil-water displacement. Porosity, absolute permeability, effective permeability, relative permeability, and oil recovery were among the basic parameters that were used to evaluate the accuracy and performance of pore geometry impact and to compare it with earlier study. The findings of this work showed that, in comparison to previous researches, the experimental work using reconstituted matrix estimates and evaluate pore geometry and grain distribution effects on oil-water relative permeability and oil recovery under laboratory conditions with the highest accuracy. Moreover, different grain size samples flooding experiments were conducted to prove how the suggested reconstituted matrix affected the samples' oil recovery and relative permeability.

Nomenclature

S_{wi}	irreducible water saturation (%)
V_{or}	residual oil volume (ml)
OOIP	original oil in place (m)
V_r	recovered oil volume (ml).
ϕ	porosity (%)
m_s	saturated mass (g)
m_d	dry mass (g)
Q	flow rate of the phase through the sample (cm^3/s)
K_a	absolute permeability of the flowing phase (Darcy)
A	fluid passage section (cm^2)
μ	fluid viscosity (cP)
L	length of the sample (cm)
K_{ao}	absolute permeability of oil (Darcy)
K_{aw}	absolute permeability of water (Darcy)
Q_o	volumetric oil flow rate (cm^3/s)
Q_w	volumetric water flow rate (cm^3/s)
K_{eo}	effective permeability of oil (mD)
K_{ew}	effective permeability of water (mD)
μ_o	oil viscosity (cP)
μ_w	water viscosity (cP)
K_{ro}	relative permeability of oil (Darcy)
K_{rw}	relative permeability of water respectively (Darcy)
L	sample length (cm)

Greek letters

ΔP	differential pressure (atm)
ΔP_w	differential pressure of water (atm)
ΔP_o	differential pressure of oil (atm)

References

- [1] Blunt MJ. Multiphase flow in permeable media: A pore-scale perspective. Cambridge university press, 1st edition (March 27, 2017): p, 500
- [2] Zakaria A, Djamila B, Souad HM, Hamid L, Mustapha M. Laboratory Investigation of the Water Trapping Phase Phenomenon in Powdered Cores Based on Reservoir Rock Cuttings and Remediation by a New Alcoholic-Treated Water Mixture. *Petroleum & Coal*, 2024; 66 (3): 1099-1106
- [3] Zhang G, Foroughi S, Raeini AQ. The impact of bimodal pore size distribution and wettability on relative permeability and capillary pressure in a microporous limestone with uncertainty quantification. *Advances in Water Resources*, 2023; 171: 104-352.
<https://doi.org/10.1016/j.advwatres.2022.104352>
- [4] Blunt MJ, Bijeljic B, Dong Hu. Pore-scale imaging and modelling. *Advances in Water resources*, 2013; 51: 197-216. <https://doi.org/10.1016/j.advwatres.2012.03.003>

- [5] Wildenschild D, Sheppard AP. X-ray imaging and analysis techniques for quantifying pore-scale structure and processes in subsurface porous medium systems. *Advances in Water resources*, 2013; 51: 217-246. <https://doi.org/10.1016/j.advwatres.2012.07.01>
- [6] Arns CH, Bauguet F, Limaye A. Pore-scale characterization of carbonates using X-ray microtomography. *Spe Journal*, 2005; 10(04): 475-484. <https://doi.org/10.2118/90368-PA>
- [7] Bultreys T van Hoorebeke L, Cnudde V. Multi-scale, micro-computed tomography-based pore network models to simulate drainage in heterogeneous rocks. *Advances in Water resources*, 2015; 78: 36-49. <https://doi.org/10.1016/j.advwatres.2015.02.003>
- [8] Pak T, Butler IB, Geiger S. Multiscale pore-network representation of heterogeneous carbonate rocks. *Water Resources Research*, 2016; 52(7): 5433-5441. <https://doi.org/10.1002/2016WR018719>
- [9] Gao Y, Lin Q, Bijeljic B. X-ray microtomography of intermittency in multiphase flow at steady state using a differential imaging method. *Water resources research*, 2017; 53(12): 10274-10292. <https://doi.org/10.1002/2017WR021736>
- [10] Lin Q, Bijeljic B, Pini R. Imaging and measurement of pore-scale interfacial curvature to determine capillary pressure simultaneously with relative permeability. *Water Resources Research*, 2018; 54(9): 7046-7060. <https://doi.org/10.1029/2018WR023214>
- [11] Alhammedi AM, Gao Y, Akai T. Pore-scale X-ray imaging with measurement of relative permeability, capillary pressure and oil recovery in a mixed-wet micro-porous carbonate reservoir rock. *Fuel*, 2020; 268: 117018. <https://doi.org/10.1016/j.fuel.2020.117018>
- [12] Lin Q, Bijeljic B, Foroughi S. Pore-scale imaging of displacement patterns in an altered-wettability carbonate. *Chemical Engineering Science*, 2021; 235: 116464. <https://doi.org/10.1016/j.ces.2021.116464>
- [13] Helmy AG, Salem SK, Elnoby Mohsen. A Study on Optimal Well Spacing for Unconventional Tight Oil Reservoirs Utilizing 3D Reservoir Simulation. *Petroleum & Coal*, 2024; 66(1): 176-191.
- [14] Kerunwa A, Izuwa NCh, Dike ChF, Okereke NU, Udeagbara SG, Obibuike JU, Emenike BUK. Review on the Utilization of Local ASP in the Niger-Delta for Enhanced Oil Recovery. *Petroleum & Coal*, 2024; 66(1): 256-275
- [15] Raeini AQ, Giudici LM, Blunt MJ. Generalized network modelling of two-phase flow in a water-wet and mixed-wet reservoir sandstone: uncertainty and validation with experimental data. *Advances in Water Resources*, 2022; 164: 104194. <https://doi.org/10.1016/j.advwatres.2022.104194>
- [16] Adjou Z, Dobbi A, Hamid L. Experimental investigation of the water bypass phenomenon in light oil reservoirs using a glass micromodel and sand cores with a hydrophobic material. *Petroleum Science and Technology*, 2024; 42(18): 2358-2371. <https://doi.org/10.1080/10916466.2022.2164774>

To whom correspondence should be addressed: Zakaria Adjou, Department of Hydrocarbon Production, KasdiMerbah University, Ouargla, Algeria, E-mail: dradjou2019@gmail.com